Photophysical Properties of Long Rodlike *Meso*−*Meso*-Linked Zinc(II) Porphyrins Investigated by Time-Resolved Laser Spectroscopic Methods

Yong Hee Kim,[†] Dae Hong Jeong,[†] Dongho Kim,*[,†] Sae Chae Jeoung,[‡] Hyun Sun Cho,[§] Seong Keun Kim,[§] Naoki Aratani,[||] and Atsuhiro Osuka*[,||]

Contribution from the Center for Ultrafast Optical Characteristics Control, Department of Chemistry, Yonsei University, Seoul 120-749, Korea, Korea Research Institute of Standards and Science, Taejon 305-600, Korea, Department of Chemistry, Seoul National University, Seoul 151-742, Korea, and Department of Chemistry, Graduate School of Science, Kyoto University, Kyoto 606-8502, Japan

Received March 20, 2000. Revised Manuscript Received October 11, 2000

Abstract: The molecular design of directly *meso*−*meso*-linked porphyrin arrays as a new model of light-harvesting antenna as well as a molecular photonic wire was envisaged to bring the porphyrin units closer for rapid energy transfer. For this purpose, zinc(II) 5,15-bis(3,5-bis(octyloxy)phenyl)porphyrin (Z1) and its directly *meso*−*meso*-linked porphyrin arrays up to Z128 (Z*n*, *n* represents the number of porphyrins) were synthesized. The absorption spectra of these porphyrin arrays change in a systematic manner with an increase in the number of porphyrins; the high-energy Soret bands remain at nearly the same wavelength (413−414 nm), while the low-energy exciton split Soret bands are gradually red-shifted, resulting in a progressive increase in the exciton splitting energy. The exciton splitting is nicely correlated with the values of $\cos[\pi/(N + 1)]$ according to Kasha's exciton coupling theory, providing a value of 4250 cm^{-1} for the exciton coupling energy in the S_2 state. The increasing red-shifts for the Q-bands are rather modest. The fluorescence excitation anisotropy spectra of the porphyrin arrays show that the photoexcitation of the high-energy Soret bands exhibits a large angle difference between absorption and emission dipoles in contrast with the photoexcitation of the low-energy exciton split Soret and Q-bands. This result indicates that the high-energy Soret bands are characteristic of the summation of the individual monomeric transitions with its overall dipole moment deviated from the array chain direction, while the low-energy Soret bands result from the exciton splitting between the monomeric transition dipoles in line with the array chain direction. From the fluorescence quantum yields and fluorescence lifetime measurements, the radiative coherent length was estimated to be 6−8 porphyrin units in the porphyrin arrays. Ultrafast fluorescence decay measurements show that the $S_2 \rightarrow S_1$ internal conversion process occurs in less than 1 ps in the porphyrin arrays due to the existence of exciton split band as a ladder-type deactivation channel, while this process is relatively slow in Z1 (∼1.6 ps). The rate of this process seems to follow the energy gap law, which is mainly determined by the energy gap between the two Soret bands of the porphyrin arrays.

Introduction

Recently, considerable attention has been focused on the synthesis of monodisperse macromolecular rods of precise length and constitution in light of their potential application as molecular-scale electronics, optical devices, sensors, and solar energy conversion.[1−3] Sufficiently long such molecules can be used for a construction of nanoarchitectures. Such oligomers can also offer a good opportunity for a systematic study on structure−property relationships which will be useful for predicting specific information on the electronic, photonic, and morphological properties of their corresponding polydisperse high molecular weight analogues. Molecular rods may be used to position two active centers at a known distance apart and connect them by a medium of known structure.[3] The degree of interaction between the centers must depend on the electronic structure of the rod and thus can be large for the rods of small HOMO−LUMO energy gaps.

Requirements for molecular photonic wires are (1) ample electronic interactions between the neighboring pigments which facilitate rapid energy transfer, (2) a lack of any energy sink which disrupts the energy flow along the array, (3) well-defined molecular geometry, and (4) sufficient molecular length that is enough for linkage of a microelectrode.

In recent years, a variety of molecular modules have been employed as a construction element of supramolecular rods. Among these, porphyrins are one of the most attractive building blocks due to their desirable characteristics such as rigid planar geometry, high stability, intense electronic absorption, and small HOMO−LUMO energy gap.[4−9] Recently, we have succeeded

* To whom correspondence should be addressed.
[†] Yonsei University.
[‡] Korea Research Institute of Standards and Science.
[§] Seoul National University.
[||] Kyoto University.

(1) Wagner, R. W.; Lindsey, J. S.; Seth, J.; Palaniappan, V.: Bocian, D. F. *J. Am. Chem. Soc.* **1996**, *118*, 3996.
(2) Wagner, R. W.; Lindsey, J. S. *J. Am. Chem. Soc.* **1994**, *116*, 9759.
(3) Martin, R. E.; Diederich, F. *Angew. Chem., Int. Ed.* **1999**, *38*, 1350.
(4) Ponomarev, G. V.; Borovkov, V.; Sugiura, K.; Sakata, Y.; Shul'ga, A. *Tetrahedron Lett.* **1993**, *34*, 2153. (b) Senge, M. O.; Gerzevske, K.; Vicente, M.; Forsyth, T.; Smith, K. M. *Angew. Chem., Int. Ed. Engl.* **1993**, *32*, 750. (c) Ponomarev, G.; Borovkov, V.; Shul'ga, A.; Sakata, Y. *J. Chem.*

10.1021/ja0009976 CCC: $20.00
Published on Web 12/14/2000

Chart 1

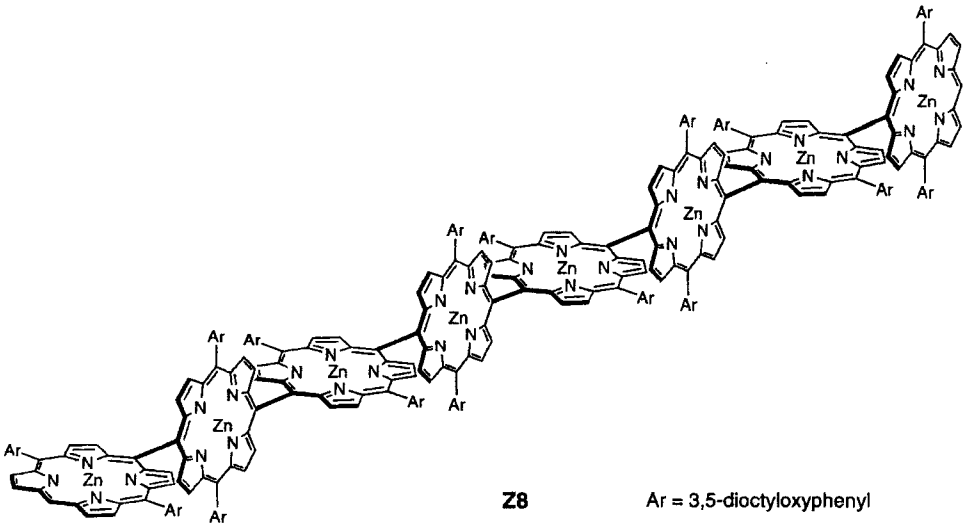

in preparation of *meso*−*meso* directly linked zinc(II) porphyrin arrays up to 128-mer (Z128) in a discrete manner by repeated Ag(I)-salt-promoted dimerization reaction.[9]

These arrays are appealing owing to the unprecedented giant molecular size, the expected simple rodlike molecular shape, and the repeated regular arrangement of porphyrin rings with large electronic interactions. These properties are also interesting in view of a potential use as photonic molecular wire, since (1) on the basis of the linear molecular shape the whole molecular length can be easily predicted by the number of porphyrins (8.35 Å per one porphyrin unit), (2) the large electronic interactions between the neighboring porphyrins are favorable for rapid excitation-energy hopping, and (3) each porphyrin unit is expected to retain its individual character presumably due to the orthogonal geometry, thus minimizing formation of any energy sink which will disrupt the energy flow along the arrays.

Here as an initial step of studies on the photophysical properties of the arrays, a series of the *meso*−*meso*-linked Zn(II) porphyrin arrays (Chart 1) including up to Z128 has been extensively studied by the steady-state absorption and fluorescence spectra, the steady-state absorption/fluorescence anisotropy, the resonance Raman spectroscopic measurement, the fluorescence anisotropy decay measurement, the fluorescence lifetime measurement, and the femtosecond fluorescence upconversion measurement. Through these studies, we have attempted to reveal the electronic absorption characteristics from the ground state to the respective excited states, the internal conversion dynamics from the upper excited state to the lowest excited state, the relative orientation of the absorption versus the fluorescence emission, the rotational diffusion motion along with the decay of the lowest excited emitting states, and the coherent length in the lowest excited state.

Experimental Methods

Zinc(II) 5,15-bis(3,5-bis(octyloxy)phenyl)porphyrin (Z1) (we denote the *meso*−*meso*-coupled Zn(II) porphyrin arrays as Z*n*, where *n* represents the number of porphyrins) and its *meso*−*meso*-linked porphyrins from dimer (Z2) to Z128 oligomer were synthesized through repetitive Ag(I)-promoted *meso*−*meso* coupling reactions. The recycling GPC−HPLC was used for product separation. MALDI-TOF mass and ^{1}H NMR spectra were employed for product characterization.[9] The spectroscopic grade tetrahydrofuran and toluene were used as solvents for all experiments. The absorption spectra were recorded by using a Varian Cary 3 spectrophotometer, and fluorescence measurements were made on a scanning SLM-AMINCO 4800 spectrofluorometer, which makes possible to obtain the corrected spectra using rhodamine B as a quantum counter. Steady-state fluorescence anisotropy spectra were obtained by changing the detection polarization on fluorescence path parallel or perpendicular to the polarization of the exciting light. Then anisotropy values were calculated as follows:

$$r = \frac{I_{VV} - GI_{VH}}{I_{VV} + 2GI_{VH}}$$

where I_{VV} (or I_{VH}) is the signal intensity when the excitation light is vertically polarized and only the vertically (or horizontally) polarized portion of fluorescence is detected, denoting that the subscripts stand for excitation and detection polarization, respectively. The factor G is defined by I_{HV}/I_{HH} which is equal to the ratio of the sensitivities of the detection system for vertically and horizontally polarized light.

The picosecond time-resolved fluorescence experiments were carried out by using time-correlated single photon counting (TCSPC) method.[10] The picosecond excitation pulses at 563 nm were obtained from a cavity-dumped picosecond dye laser (Coherent 702) synchronously pumped by a mode-locked Nd:YAG laser (Antares 76-s). The cavity-dumped beam from the dye laser has 2 ps pulse width and an average power of ca. 40 mW at 3.8 MHz dumping rate when rhodamine 6G for gain dye was used. The excitation pulses at 410 nm were obtained from a femtosecond Ti:sappahire laser (Coherent, MIRA) with an average power of 600 mW at 820 nm. The pump pulses at desired

Soc., Chem. Commun. **1994**, 1927. (d) Senge, M. O.; Vicente, M.; Gerzevske, K.; Forsyth, T.; Smith, K. M. *Inorg. Chem.* **1994**, *33*, 5625. (e) Higuchi, H.; Takeuchi, M.; Ojima, J. *Chem. Lett.* **1996**, 593. (f) Lin, V. S.-Y.; DiMagno, S. G.; Therien, M. J. *Science* **1994**, *264*, 1105. (g) Lin, V. S.-Y.; Therien, M. J. *Chem.−Eur. J.* **1995**, *1*, 645. (h) Arnold, D. P.; Nitschinsk, L. *Tetrahedron* **1992**, *48*, 8781. (I) Anderson, H. L. *Inorg. Chem.* **1994**, *33*, 972. (j) Arnold, D. P.; Nitschinsk, L. *Tetrahedron Lett.* **1993**, *34*, 693. (k) Vicente, M. G. H.; Smith, K. M. *J. Org. Chem.* **1991**, *56*, 4407.

(5) Osuka, A.; Liu, B.-L.; Maruyama, K. *Chem. Lett.* **1993**, 949. (b) Burrell, A. K.; Officer, D.; Reid, D. *Angew. Chem., Int. Ed. Engl.* **1995**, *34*, 900. (c) Osuka, A.; Maruyama, K.; Yamazaki, I.; Tamai, N. *Chem. Phys. Lett.* **1990**, *165*, 392. (d) Osuka, A.; Maruyama, K.; Mataga, N.; Asahi, T.; Yamazaki, I.; Tamai, N. *J. Am. Chem. Soc.* **1990**, *112*, 4958.

(6) Yang, S. I.; Lammi, R. K.; Seth, J.; Riggs, J. A.; Arai, T.; Kim, D.; Bocian, D. F.; Holten, D.; Lindsey, J. S. *J. Phys. Chem. B* **1998**, *102*, 9426.

(7) Osuka, A.; Shimidzu, H. *Angew. Chem., Int. Ed. Engl.* **1997**, *36*, 135. (b) Yoshida, N.; Shimidzu, H.; Osuka, A. *Chem. Lett.* **1998**, 55. (c) Nakano, A.; Osuka, A.; Yamazaki, I.; Yamazaki, T.; Nishimura, Y. *Angew. Chem., Int. Ed. Engl.* **1998**, *37*, 3023.

(8) Cho, H. S.; Song, N. W.; Kim, Y. H.; Jeoung, S. C.; Hahn, S.; Kim, D.; Kim, S. K.; Yoshida, N.; Osuka, A. *J. Phys. Chem. A* **2000**, *104*, 3287.

(9) Aratani, N.; Osuka, A.; Kim, Y. H.; Jeong, D. H.; Kim, D. *Angew. Chem., Int. Ed.* **2000**, *39*, 1458.

(10) Lee, M.; Kim, D. *J. Opt. Soc. Korea* **1990**, *1*, 52.

wavelength were generated by frequency doubling with a β-BBO crystal. The emission was collected at a 45° angle with respect to the excitation laser beam by 5- and 25-cm focal length lenses, focused onto a monochromator (Jobin-Yvon H*R*320), and detected with a microchannel plate photomultiplier tube (Hamamatsu R2809U). The signal was amplified by a wideband amplifier (Philip Scientific), sent to a Quad constant fraction discriminator (Tennelec), a time-to-amplitude converter (Tennelec), a counter (Ortec), and a multichannel analyzer (Tennelec/Nucleus), and stored in a computer. The time-dependent anisotropy decay was obtained by using the polarizer and depolarizer before the detection system.

The ground-state resonance Raman spectra of the porphyrin arrays were obtained by photoexcitation using six lines (457.9, 476.5, 488.0, 496.5, 501.7, and 514.5 nm) of a CW Ar ion laser (Coherent INNOVA 90). These lines correspond to the low-energy exciton split Soret bands of the porphyrin arrays. Raman scattering signals were collected in a 90° scattering geometry and detected by a 1-m double monochromator (ISA Jobin-Yvon U-1000) equipped with a thermoelectrically cooled photomultiplier tube (Hamamatsu R943-02).[11] For excitation at the high-energy exciton split Soret bands of the porphyrin arrays located at ~415 nm, a 416 nm line was generated by the hydrogen Raman shifting of the third harmonics (355 nm) from a nanosecond Q-switched Nd:YAG laser. The Raman spectra were recorded by a single pass spectrometer (ISA Jobin-Yvon HR640) with a gated intensified charge-coupled device (CCD, Princeton Instruments IRY700) detector and a pulse generator (Princeton Instruments FG100). As a Raman cell, a modified Pasteur pipet whose end has a tiny capillary tube attached was used in order to make sample solution flow slowly to minimize its consumption and photodecomposition by the cw laser excitation.

The light source for fluorescence up-conversion measurement[12] was a mode-locked Ti:sapphire laser (Coherent, MIRA-900F) pumped by a intracavity frequency-doubled cw Nd:YVO_4 laser (Coherent, Verdi) with an average power of 550 mW and ~120 fs pulse width at 800 nm. The second harmonic pulses (400 nm, 90 mW) were generated by using a β-BBO (1 mm thick) crystal. The residual fundamental pulses after the dichroic mirror were used as the gate pulses for the up-conversion of fluorescence. The time interval between the fluorescence and gate pulses was controlled by a delay stage equipped with a corner cube gold retro-reflector (Coherent, 2 in. diameter) for traveling the gated pulse. The excitation laser beam was focused onto the sample by using a 5 cm focal length aluminum-coated parabolic mirror. And its power was controlled by using a variable neutral density filter. The fluorescence is collected and focused onto a β-BBO (1 mm thick, type-I) crystal for the up-conversion by using an aluminum-coated parabolic mirror (Coherent, 5 and 20 cm in focal lengths). A cutoff filter (Schott Glass Filter Co., GG475, 3 mm thick) was placed between collimating and focusing mirrors to remove the transmitted pump pulse. Up-converted signals were focused onto the entrance slit of a 15 cm focal length monochromator (IBH, 5000M) after passing through a UV band-pass filter (Schott Glass Filter Co., UG11). The signal was detected by a head-on type photomultiplier tube (Hamamatsu, model 3235) with a gated photon counter (Stanford Research Systems, SR400). The gated photon counter was interfaced with a personal computer which controls the delay stage. The full width at half-maximum value of the cross-correlation trace between the excitation and gate pulses was estimated to be ~300 fs, which determines the time resolution of the fluorescence up-conversion measurements.

Results

Steady-State Absorption and Fluorescence Anisotropy Decay. The absorption spectra of the directly linked Zn(II) porphyrin arrays normalized at ca. 413 nm which corresponds to the high-energy Soret bands are shown in Figure 1a. As reported previously,[7,9] the *meso*−*meso*-coupled arrays displayed split Soret bands due to exciton coupling. With an increase in the number of porphyrin units, the Soret band at low energy is shifted to longer wavelength, while the Soret band at shorter wavelength remains nearly at the same wavelength (ca. 413 nm), resulting in a progressive increase in the splitting energy. The relative intensities of split Soret bands also depend on the number of porphyrin units; the intensity of longer wavelength bands becomes increasingly stronger relative to that at shorter wavelength. On the other hand, the spectral shifts in the Q-band region are modest with gradual increase in intensity.

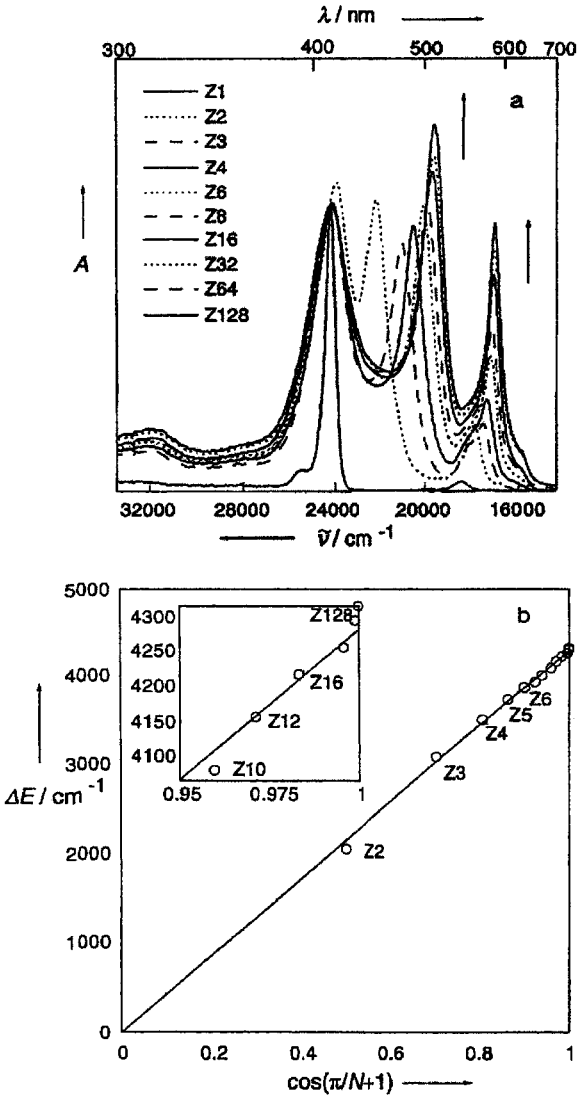

Figure 1. A series of ground-state absorption spectra of the porphyrin arrays in THF (a) and the plot of the exciton splitting energy as a function of the number of porphyrin units in the arrays (b).

The systematic spectral changes of the Soret bands can be explained by the simple point−dipole exciton coupling theory developed by Kasha.[13] The Soret band of Zn(II) porphyrin has two perpendicular components of B_x and B_y as depicted in Scheme 1. In a simple monomer, they are degenerate, but in a porphyrin dimer they couple differently. In the case of Z2, only B_x transitions are parallel, and other dipole interactions should be zero for an averaged perpendicular conformation of Z2 (Scheme 1). Unperturbed Soret transitions observed at ca. 413 nm for all the arrays (Z2−Z128) suggest an orthogonal conformation and vice versa. And these bands become broader

(11) Hwang, Y. N.; Park, S. H.; Kim, D. *Phys. Rev. B* **1999**, *59*, 299.
(12) Takeuchi, S.; Tahara, T. *J. Phys. Chem. A* **1997**, *101*, 3052.

(13) The dipole−dipole approximation led to satisfactory analysis as described in the text. But in the close proximity of the *meso*−*meso*-coupled porphyrin arrays with a center-to-center distance of ca. 8.4 Å. We have to consider multipole interactions. Kasha, M.; Rawls, H. R.; El-Bayoumi, M. A. *Pure Appl. Chem.* **1965**, *11*, 371.

Scheme 1

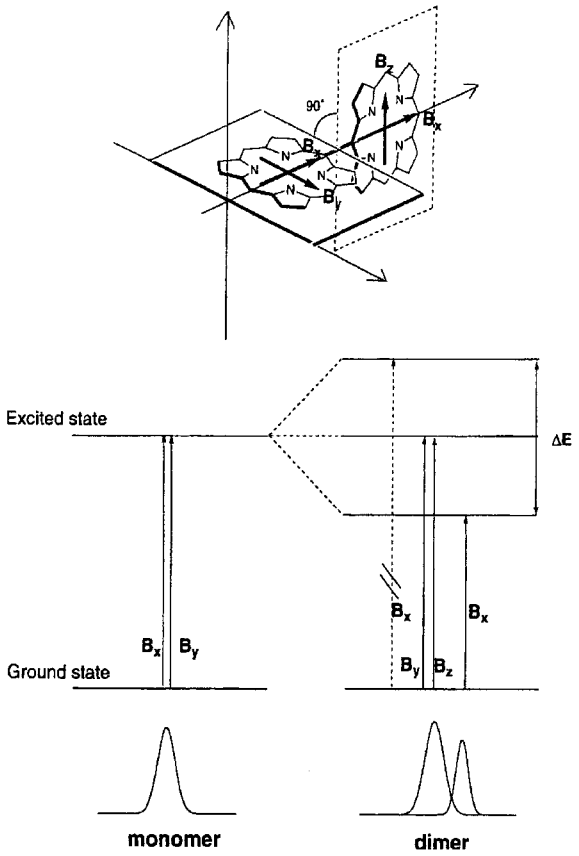

as the porphyrin arrays become longer, indicating the increasing conformational heterogeneities caused by the dihedral angle distribution, aggregate formation, and partial insolubility, if any, of longer arrays. Transitions are allowed to the lower energy of the two B_x states and the two unperturbed transitions B_y and B_z. Thus, the Soret band of Z2 is split into a red-shifted B_x component and unperturbed B_y, B_z components (Scheme 1). According to the exciton coupling theory, eq 1 predicts the relationship of the splitting energy of the neighboring porphyrin units, ΔE_0,

$$\Delta E_0 = \frac{\mu^2}{2\pi\epsilon_0 R^3} \tag{1}$$

where μ is the transition dipole moment and R is the center-to-center chromophore distance. The splitting energy (ΔE) for larger arrays should be given by eq 2,

$$\Delta E = \Delta E_0 \cos[\pi/(N+1)] \tag{2}$$

where N represents the number of chromophores. The splitting energy ΔE can be determined by doubling the observed energy difference between the red-shifted B_x band and the unpertubed $B_{y,z}$ band. When ΔE data were plotted to eq 2, we obtained a straight line with a slope of $E_0 = 4250$ cm^{-1} (Figure 1b). The observed linear relationship indicates that the absorption spectral shapes are actually influenced by the number of porphyrin units and the constituent porphyrin pigments are aligned in a regular arrangement in the series. Some deviation from the linearity, however, was observed in the region of the very long arrays. Figure 2 shows the absorption spectra of the arrays with absolute intensity, which may be helpful for recognizing the high absorptivity of the long arrays such as Z64. As the number of

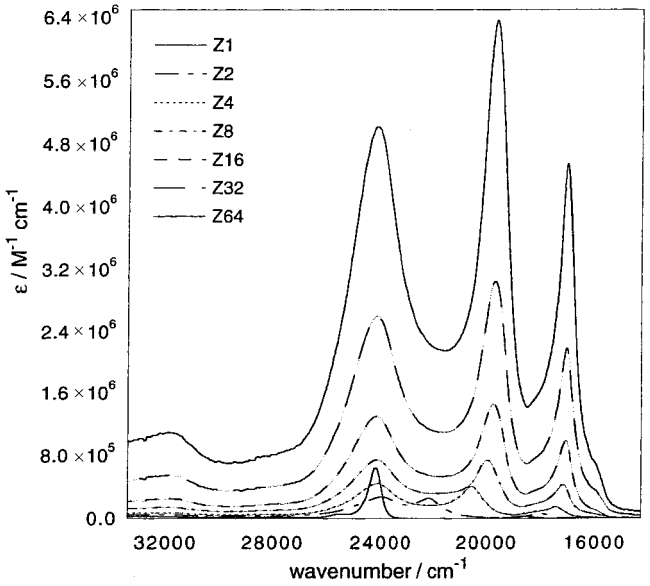

Figure 2. A series of extinction coefficient spectra of the porphyrin arrays up to Z64 in THF.

porphyrin units increases in the porphyrin arrays, the extinction coefficients are much enhanced up to $>10^6$ M^{-1} cm^{-1} for Z64 covering almost entire visible region. The large extinction coefficients as well as the wide spectral coverage in longer porphyrin arrays provide a prospect that the directly linked porphyrin arrays can be candidates as the artificial light harvesting complexes to capture a wide range of the incident visible light efficiently.

The steady-state fluorescence spectra of the porphyrin arrays according to the relative intensity scale are displayed in Figure 3. Z1 exhibits the two-peak emission (584 and 633 nm) characteristic of Zn(II) porphyrin, and Z2 exhibits a red-shifted and broader fluorescence spectrum. The fluorescence spectra of the longer arrays (Z3−Z128) are observed in nearly the same region as the two bands at ca. 15 600 cm^{-1} (640 nm) and ca. 15 000 cm^{-1} (667 nm). The relative fluorescence quantum yields determined with respect to $\phi_F = 0.03$ of $Zn^{II}TPP$ increase up to Z16 and then decrease with the increase of the number of porphyrin units.

To obtain information on the relative orientation between absorption and emission dipoles of the porphyrin arrays, we have measured the fluorescence excitation anisotropy spectra in toluene (Figure 4).[14] The fluorescence excitation polarization of the monomeric porphyrin Z1 is almost 1/7 regardless of the excitation wavelength, which is typical when both the absorption and emission oscillators are degenerate and polarized in the same plane. In the cases of porphyrin arrays, however, it is noteworthy that we obtained negative anisotropy values in the fluorescence excitation anisotropy spectra around 413 nm which corresponds to the high-energy Soret band. The limiting negative anisotropy value of approximately −0.1 as the number of porphyrin units increases in the arrays indicates a relatively large angle displacement between absorption and emission dipoles upon photoexitation at ∼413 nm, though this value is still smaller than the orthogonal orientation anisotropy value of −0.2. The anisotropy values above ∼450 nm for this series of porphyrin arrays are positive, and the difference between the anisotropy values of around 413 nm and the entire visible region becomes larger as the number of porphyrin rings increases. The limiting

(14) Cantor, C. R.; Schimmel, P. R. *Biophysical Chemistry Part II: Techniques for the Study of Biological Structure and Function*; W. H. Freeman and Co.: San Francisco, CA, 1980.

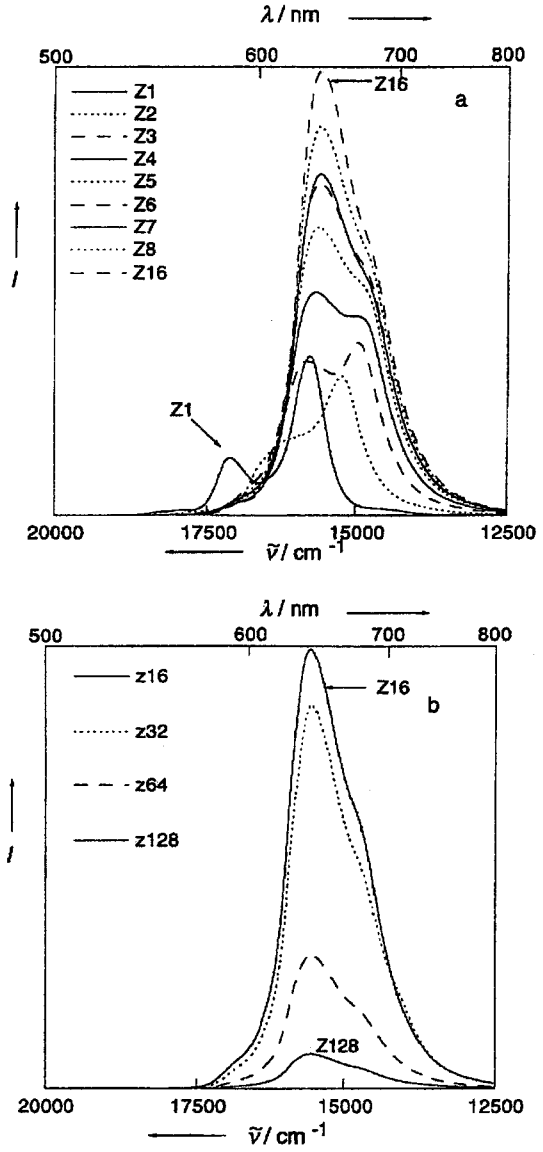

Figure 3. A series of steady-state fluorescence spectra of the porphyrin arrays in THF according to the relative intensity scale.

positive anisotropy value of ~0.3 in longer arrays, which is still slightly smaller than 0.4 for the perfect in-plane orientation between absorption and emission dipoles, indicates a relatively small angle displacement between absorption and emission dipoles upon photoexcitation at the low-energy exciton split Soret and Q-bands. Furthermore, the similar positive anisotropy values of the porphyrin arrays in the regions of the low-energy exciton split Soret band and Q-band indicate that the relative orientation between absorption and emission dipoles is in the same direction for these two transitions.

The fluorescence anisotropy decay, $r(t)$, offers detailed information on the diffusive motions of the fluorophore.[15,16] In general $r(t)$ exhibits *multi*exponential decay rates due to anisotropic rotations with respect to its three molecular axes. Thus, upon increase of the number of porphyrin molecules, these oligomers become nonsymmetric, so one does not expect equal rotational rates in all directions. As the overall molecular shape

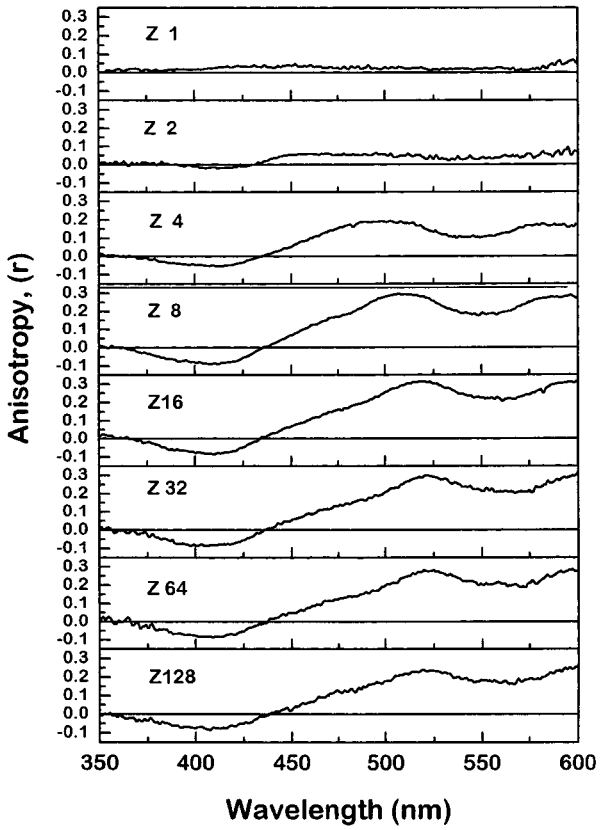

Figure 4. A series of steady-state fluorescence excitation anisotropy spectra of the porphyrin arrays in THF.

Table 1. Summary of Various Photophysical Properties of Porphyrin Arrays Such as Fluorescence Lifetme (τ), Relative Fluorescence Quantum Yields (Φ_f), Natural Radiative Lifetime (τ_0), Initial Anisotropy Values (r_0), Rotational Diffusion Time constants (Φ), and Anisotropy Values (r)

compd	Φ_f	τ (ns)[a]	τ_0	Φ (ns)	r_0	r
Z1	0.022	2.64 ± 0.04	120	0.45 ± 0.04	0.05	0.007 (0.01)[b]
Z2	0.029	1.94 ± 0.03	67	1.04 ± 0.05	0.09	0.03 (0.029)
Z3	0.045	1.83 ± 0.03	41	1.51 ± 0.05	0.24	0.09 (0.11)
Z4	0.060	1.75 ± 0.02	29	2.54 ± 0.02	0.27	0.163 (0.160)
Z5	0.073	1.71 ± 0.02	23	2.61 ± 0.02	0.32	0.19 (0.19)
Z6	0.081	1.66 ± 0.02	20	3.19 ± 0.3	0.32	0.21 (0.22)
Z7	0.081	1.62 ± 0.01	20	4.29 ± 0.3	0.34	0.25 (0.22)
Z8	0.090	1.60 ± 0.01	18	5.01 ± 0.46	0.35	0.24 (0.22)
Z16	0.097	1.54 ± 0.01	16	>10[c]	0.26	0.23 (0.23)
Z32	0.085	1.2 ± 0.01	14	>10[c]	0.23	0.22 (0.21)
Z64	0.042	0.25 ± 0.01	6	> 10[c]	0.17	0.17 (0.18)
Z128	0.008	0.12 ± 0.02	15	>10[c]	0.12	0.17 (0.17)

[a] Probed at the fluorescence maximum position with photoexcitation at 570 nm. [b]Estimated from steady-state polarized excitation spectra. [c] The time window of our TCSPC system is 16 ns. Accordingly, only a rough estimation is given for the rotational diffusion times for longer porphyrin arrays.

is elongated into the long axis of the arrays in the order of increasing porphyrin units, the molecular rotation perpendicular to the long axis should experience more restriction from the surrounding solvent molecules to exhibit slower rotational diffusion rate. In addition, the in-plane rotational contribution to the overall rotational diffusion motion is less significant upon increasing the number of porphyrin units, and consequently the overall anisotropic decay rate becomes slower (Table 1).

We also measured the fluorescence lifetimes of the porphyrin arrays in toluene by using the time-correlated single photon counting method. After the formation of the vibrationally ground S_1 state, the relaxation processes decaying to the ground state

(15) Agranovich, V. M.; Galanin, M. D. *Electronic Excitation Energy Transfer in Condensed Matter*; North-Holland: Amsterdam, 1982. (b) Kim, Y. R.; Share, P.; Pereira, M.; Sarisky, M.; Hochstrasser, R. M. *J. Chem. Phys.* **1989**, *91*, 7557.

(16) Lakowicz, J. R. *Principles of Fluorescence Spectroscopy*; Plenum Press: New York and London, 1983.

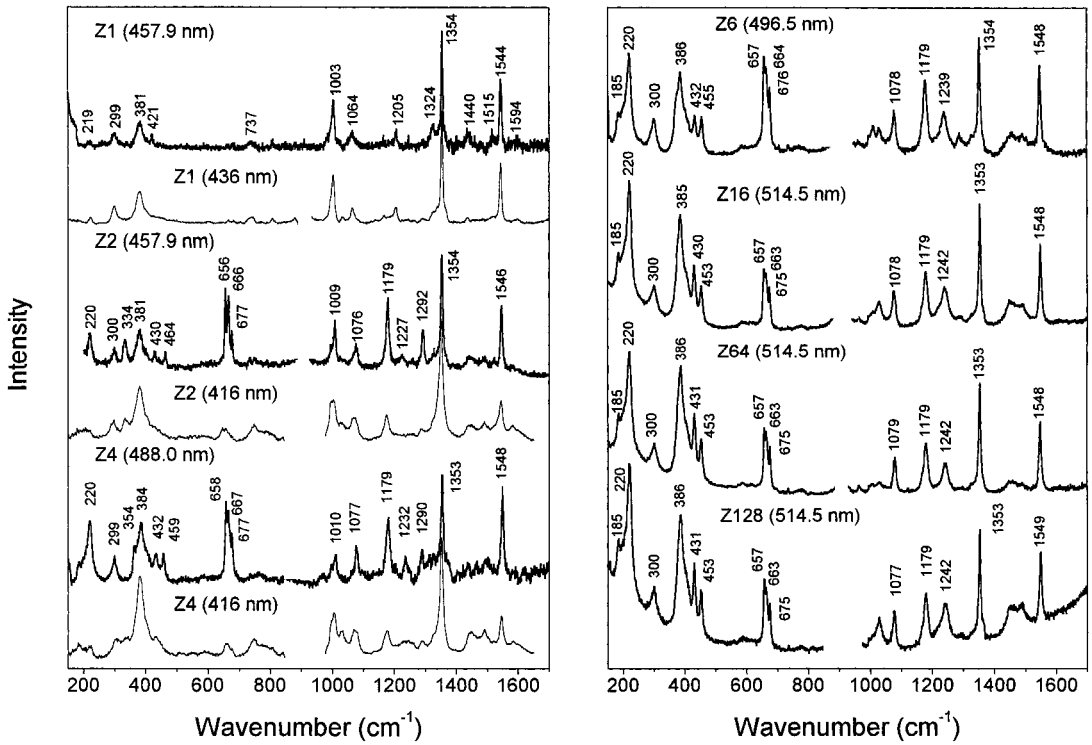

Figure 5. A series of ground-state RR spectra of the porphyrin arrays from Z1 to Z128. For Z1, the thick solid line represents the RR spectrum obtained by photoexcitation with 457.9 nm line and the thin solid line the RR spectrum by photoexcitation at 436 nm. For Z2 and Z4, the thick solid lines represent the RR spectra obtained by photoexcitation in resonance with the low-energy exciton split Soret bands and the thin solid lines are the RR spectra obtained by photoexcitation at high-energy Soret bands at ~416 nm. The RR spectra for Z6, Z16, Z64, and Z128 were obtained by photoexciation in resonance with the low-energy exciton split Soret bands.

appear as fluorescence decays with the lifetime of 2.64 ns in the monomeric porphyrin Z1.[17] As the number of porphyrin units increases in the arrays, the fluorescence lifetimes gradually decrease to exhibit asymptotic feature. It is also noteworthy that the fluorescence decay becomes nonexponential in longer arrays especially above Z32 probably due to the increased conformational heterogeneity in conformers and aggregate formation (or partially insoluble arrays) in longer arrays. Thus the average decay time constants are regarded as the fluorescence lifetimes for the longer porphyrin arrays. The overall photoexcitation dynamics occurring in these porphyrin arrays are summarized in Table 1.

Resonance Raman Spectroscopic Measurements. Ground-state RR spectra of Zn(II) porphyrin arrays were obtained by photoexcitation at their low-energy exciton split Soret bands; for instance, 457.9, 476.5, 488.0, 496.5, and 501.7 nm for Z2, Z3, Z4, Z6, and Z8, respectively, and 514.5 nm for longer arrays. The Raman spectrum of Z1 was also obtained by excitation with the 457.9 nm line. Representative Raman spectra of the porphyrin arrays (Z1, Z2, Z4, Z6, Z16, Z64, and Z128) are shown in Figure 5. The Raman bands at ~1354 and ~1544 cm^{-1} in Z1, which can be assigned to the totally symmetric ν_4 and ν_2 modes, respectively, are observed at nearly the same position in each spectrum. Some distinct features, however, become manifest in the Raman spectra of the porphyrin arrays. Especially, three Raman bands at ~660 cm^{-1}, where no band is observed in Z1, show systematic decrease in their intensities as the number of porphyrin units in the arrays increases. The Raman band at ~1179 cm^{-1} shows a similar trend with an increase of porphyrin units in the arrays. On the other hand, the Raman band at 220 cm^{-1} with its shoulder at 185 cm^{-1}, which is phenyl−porphyrin *inter*-ring stretching (195 cm^{-1} in Ni(II)TPP [18]), gains its intensity with an increase of porphyrin units in the arrays. The Raman band at 381 cm^{-1} also becomes strongly enhanced with a slight blue-shift to 386 cm^{-1} with an increase of porphyrin units. The Raman band at ~1230 cm^{-1}, which is weak in Z2, gradually increases with a blue-shift to 1242 cm^{-1} with an increase of porphyrin units. The Raman bands at 1003 and 1064 cm^{-1} in Z1 are shifted to higher frequencies, and their relative intensity ratios become reverse as the number of porphyrin units in the arrays increases. Overall, a systematic change in intensity and frequency with an increase in the number of porphyrin units in the arrays indicates that there is a strong correlation between molecular structures and Raman spectra of the porphyrin arrays. The Raman band at 334 cm^{-1} in Z2 is also affected significantly in frequency. Deconvolution of the Raman bands located at approximately 400 cm^{-1} region has revealed one of the Raman bands with the gradual frequency shift from 334 cm^{-1} in Z2 to 378 cm^{-1} in longer arrays with an increase of porphyrin units in the arrays. This

(17) The side chain (Ar = 3,5-bis(octyloxy)phenyl) in the porphyrin arrays investigated in this work is different from that (Ar = 3,5-di-*tert*-butylphenyl) in the previous one,[8] although the same abbreviation for the compound such as Z*N* (*N* = the number of porphyrin units) has been used in both manuscripts. The 3,5-bis(octyloxy)phenyl group has been utilized for the enhancement of the solubility of longer porphyrin arrays, which is quite important in photophysical measurements of porphyrin arrays in solution. Thus the molecular structure and shape become slightly different, which probably results in the differences in the fluorescence lifetimes and rotational diffusion times. More specifically, the fluorescence lifetimes for Z1 are slightly different from each other (2.57 vs 2.64 ns) and the rotational diffusion times also become slower for longer side chain substituted ones (Ar = 3,5-bis(octyloxy)phenyl) (0.45 vs 0.3 ns). This trend is maintained for Z3 and Z4 as compared with the data presented in ref 8. Thus the longer side chain really improves the solubility of longer porphyrin arrays, but it does affect slightly the fluorescence lifetimes and rotational diffusion times of porphyrin arrays.

(18) Li, X.-Y.; Czernuszewicz, R. S.; Kincaid, J. R.; Su, Y. O.; Spiro, T. G. *J. Phys. Chem.* **1990**, *94*, 31.

band is suggested to originate from the vibrational mode involving the *meso*-carbon movement along the long axis of the porphyrin arrays on the basis of the normal-mode analysis of the dimer using AM1 method. Thus, this movement is likely to be increasingly damped as the number of porphyrin units increases. This effect becomes negligible especially in longer arrays because porphyrin at one end cannot effectively feel the existence of another porphyrin unit at the other end.

We have also observed the ground-state RR spectra of Zn(II) porphyrin arrays from Z1 to Z4 with excitation at their high-energy Soret bands (Figure 5).[19] The RR spectrum of Z1 is the same as that with 457.9 nm excitation. However, the overall Raman spectral features of Z2 and Z4 are very different from those with low-energy Soret band excitation. They closely resemble the RR spectrum of Z1, in which the new RR bands at 334, ~660, and 1179 cm^{-1} are weakly observed and the totally symmetric bands at 381, 1,007, 1,075, 1,352, and 1545 cm^{-1} are predominant in the RR spectrum.[20] The observation that the RR spectral features of the porphyrin arrays with excitation at both high- and low-energy Soret bands are different from each other indicates that the two Soret bands have distinctly different electronic nature even though they originate from the same monomeric Soret band.

Ultrafast Internal Conversion Processes. To investigate the internal conversion processes occurring in the porphyrin arrays, we employed the femtosecond fluorescence up-conversion technique to measure the time constant to populate the lowest excited emitting S_1 state upon photoexcitation to the higher electronic states of the porphyrin arrays. Thus, the observed rise components in the fluorescence temporal profiles are believed to arise mainly from the overall internal conversion processes to populate the emissive S_1 state after photoexcitation to the S_2 state at ~400 nm. The fluorescence temporal profiles of Z1 at the red edge of fluorescence emission after photoexcitation at around 400 nm exhibit the rise component with ~1.6 ps time constant, which corresponds to the relatively slow $S_2 \rightarrow S_1$ internal conversion process (not shown). It is already well established that the S_2 states of Zn(II) 5,10,15,20-tetraphenylporphyrin and Zn(II) 5,15-diphenylporphyrin analogues are relatively long-lived with 1−2 ps lifetimes.[21,22] Since the Z1 compound is Zn(II) 5,15-bis(3,5-bis(octyloxy)phenyl)porphyrin, the 1.6 ps lifetime of the S_2 state seems to be reasonable. Figure 6 also shows the temporal profiles of fluorescence signal in Z2, illustrating about 300 fs rise and subsequent ~20 ps decay components. The fluorescence temporal profiles of Z3 exhibit about 500 fs rise and subsequent ~20 ps rise components. As for Z4, we were able to observe a rise component with approximately 700 fs time constant, which appeared to be a saturation value for the initial rise component with an increase in the number of porphyrin units in the arrays. The following decay component with ~20 ps time constant was also found in the fluorescence temporal profile. In the case of Z8, a rise component with ~700 fs in the fluorescence temporal profiles was observed with a subsequent relatively slow rise component with ~20 ps time constant. As for longer porphyrin oligomers such as Z16, Z32, Z64, and Z128, the initial decay components with a few picoseconds time constants are clearly seen in the fluorescence decay profiles in addition to ~700 fs rise and 20−30 ps decay components as observed in Z2−Z4 and Z8 (Figure 6).[23]It is to be noted that there exists long-lived tail due to the S_1 state emission decay of the porphyrin arrays in the fluorescence temporal profiles displayed in Figure 6. This component should appear as a plateau in the time window employed in Figure 6. Thus the time constant for this slowest decay process in the porphyrin arrays was confirmed by the TCSPC technique. The initial decay components of 1−4 ps time constants in the fluorescence temporal profiles of the porphyrin arrays exhibit the photoexcitation power density dependence (not shown). Thus we suggest that these components arise from exciton−exciton annihilation processes contributed by the high density of excitons produced under high photoexcitation density illumination. The fluorescence temporal profiles for longer porphyrin arrays were obtained up to longer time delay to confirm the time constant and relative contribution of 20−30 ps decay components to the overall dynamics upon photoexcitation to the S_2 states of the porphyrin arrays (insets of Figure 6). As the photoexcitation wavelength is shifted to red, these components become manifest in the temporal profiles of fluorescence signals in the porphyrin arrays due to the photoexcitation of the heterogeneous conformers in the ground state more preferentially at a certain wavelength (not shown).

Discussion

Electronic Nature of the Exciton Split Soret Band. The absorption spectra of longer Zn(II) porphyrin arrays displayed in Figure 1 are reminiscent of water-soluble porphyrin *J*-aggregates, which exhibit sharp and red-shifted peaks below the Q- and B-bands in aqueous solution at room temperature.[24] The *J*-aggregates are characteristic of a sharp absorption band below the transition band of monomers. Intermolecular interaction between dipole moments causes the coherent delocalization of excitons over an aggregate. Thus the exciton split low-energy Soret band can be represented by the head-to-tail arrangement of the B_x transition dipoles in the porphyrin arrays as depicted in Scheme 1. On the other hand, according to the four-orbital model, the strength of the Q(0,0) transition is dictated by the energy difference between the porphyrin $a_{1u}(\pi) \rightarrow e_g(\pi^*)$ and $a_{2u}(\pi) \rightarrow e_g(\pi^*)$ one-electron promotions and is thus strongly influenced by the relative energies of the $a_{1u}(\pi)$ and $a_{2u}(\pi)$ HOMOs (vide infra). The intensity of the Q(1,0) band does not change significantly among metalloporphyrins because this band primarily derives intensity via vibronic borrowing from the strong Soret band. In Zn(II) porphyrin monomer, the Q(1,0) band is dominant. The Q-bands of the porphyrin arrays become enhanced and sharper as the number of porphyrin units increases (Figure 1). Since the Q(1,0) bands of Zn(II) porphyrins gain their intensities via vibronic coupling from the B-bands, the enhanced Q-bands of the porphyrin arrays are due to the increased vibronic coupling mainly attributed by the decreased energy gap between the exciton split low-energy B- and Q-bands in the porphyrin arrays. The sharp exciton split B- and Q-bands

(19) Greiner, S. P.; Winzenburg, J.; von Maltzan, B.; Winscom, C. J.; Moebius, K. *Chem. Phys. Lett.* **1989**, *155*, 93. (b) Fulton, R. L.; Gourterman, M. *J. Chem. Phys.* **1961**, *35*, *1059*; **1964**, *41*, 2280.

(20) Burke, J. M.; Kincaid, J. R.; Spiro, T. G. *J. Am. Chem. Soc.* **1978**, *100*, 6077. (b) Hofmann, J. A., Jr.; Bocian, D. F. *J. Phys. Chem.* **1984**, *88*, 1472. (c) Seth, J.; Palaniappan, V.; Johnson, T. E.; Prathapan, S.; Lindsey, J. S.; Bocian, D. F. *J. Am. Chem. Soc.* **1994**, *116*, 10578. (d) Nakashima, S.; Taniguchi, S.; Okada, T.; Osuka, A.; Mizutani, Y.; Kitagawa, T. *J. Phys. Chem. A* **1999**, *103*, 9184.

(21) Kobayashi, H.; Kaizu, Y. In *Porphyrins*: *Excited States and Dynamics;* Gouterman, M., Rentzepis, P., Straub, K. D., Eds.; American Chemical Society Symposium Series 321; American Chemical Society: Washington, DC, 1986; p 105.

(22) Chosrowjan, H.; Tanigichi, S.; Okada, T.; Takagi, S.; Arai, T.; Tokumaru, K. *Chem. Phys. Lett.* **1995**, *242*, 644. (b) Gurzadyan, G. G.; Tran-Thi, T.-H.; Gustavsson, T. *J. Chem. Phys.* **1998**, *108*, 385. (c) Mataga, N.; Shibata, Y.; Chosrowjan, H.; Yoshida, N.; Osuka, A. *J. Phys. Chem. B* **2000**, *104*, 4001.

(23) Kumble, R.; Palese, S.; Lin, V. S.-Y.; Therien, M. J.; Hochstrasser, R. M. *J. Am. Chem. Soc.* **1998**, *120*, 11489.

(24) Misawa, K.; Kobayashi, T. *J. Chem. Phys.* **1999**, *110*, 5844.

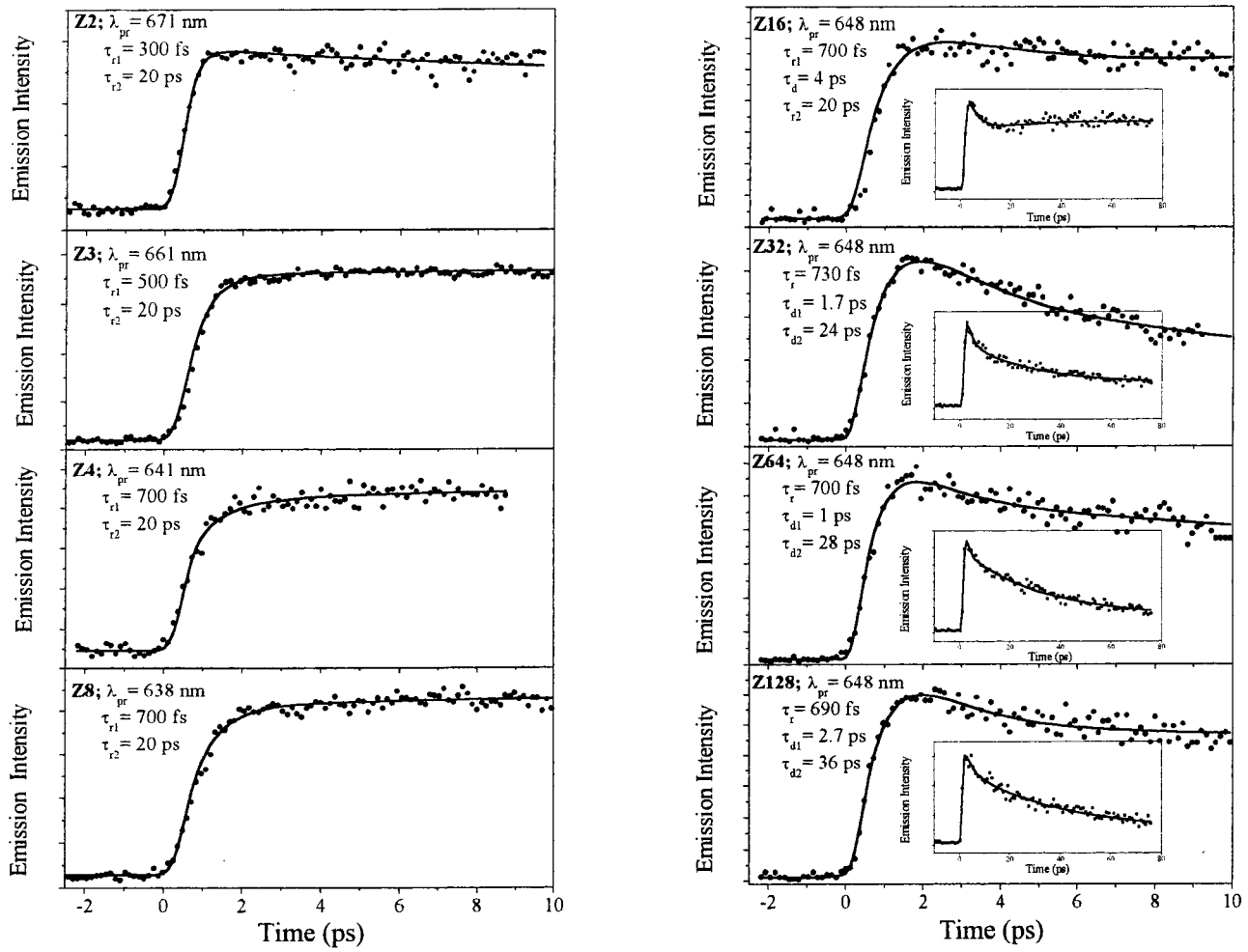

Figure 6. Fluorescence up-conversion decay profiles of the porphyrin arrays at various probe wavelengths after photoexcitation at 400 nm. The insets show the fluorescence decay profiles up to longer delay times. τ_r and τ_d represent the rise and decay time constants, respectively.

are consistent with the view of the electronic transitions of porphyrin *J*-aggregates. The orientations of the transition dipoles for low-energy exciton split B and Q-bands are the same, which is along the long axis of the porphyrin arrays as shown by the positive anisotropy values in the fluorescence excitation anisotropy spectra for these two transitions. Relatively broad B-bands at ca. 413 nm that correspond to the monomeric Soret transition suggest that there exits the conformational heterogeneities arising form the dihedral angle distribution between the adjacent porphyrin units in the porphyrin arrays.

Along with the steady-state fluorescence excitation anisotropy spectra of the porphyrin arrays, the excitation energy-dependent RR spectra reveal the different electronic nature for the two Soret bands of the porphyrin arrays (Figure 5). The RR spectra of Z2 and Z4 with an excitation at high-energy Soret bands are similar to the RR spectrum of monomer Z1. But the RR spectra of Z2 and Z4 with an excitation at their low-energy exciton split Soret bands exhibit some new RR bands, which are absent in the RR spectrum of monomer Z1. The different RR enhancement pattern in the porphyrin arrays depending on the excitation wavelength is consistent with the above arguments that the two Soret bands of the porphyrin arrays have electronic natures different from each other (Figure 7).

Superradiance Coherent Length of the Porphyrin Arrays. Cooperative spontaneous emission (superradiance) gives a signature of coherent length. As molecules radiate in phase, the radiative decay rate becomes enhanced.[25] The superradiance coherent length is defined as the ratio of the radiative decay rate of the porphyrin arrays to that of monomer. Thus this reflects the degree of excitonic intermolecular coherence.[26] The coherent length has been reported to be about four BChls units in LH1 and LH2 antenna complexes or a whole ring in LH2 850.[2,3] To estimate the coherent length in the porphyrin arrays investigated in this work, the natural radiative lifetimes are plotted in Figure 8 as a function of the number of porphyrin units in the arrays according to the relationship of $\tau_o = \tau/\Phi$, where τ_o, τ, and Φ are natural radiative lifetimes, fluorescence lifetimes, and fluorescence quantum yields of the porphyrin arrays, respectively.[27] Since the natural radiative lifetime is expected to be proportional to the radiative coherent length (*N* units) and the fluorescence lifetime ($\tau_0 = N\tau$), the crossing point value of approximately 6−8 porphyrin units in this plot seems to be the best estimation of the radiative coherence length in these porphyrin arrays. This coherence length seems longer than that in LH1 and LH2 complexes, which was estimated to be about four bacteriochlorophyll units. A slightly longer coherence length in the linear porphyrin arrays is probably due to the covalent direct linkage between the adjacent porphyrins with shorter center-to-center distance of ∼8.4 Å as compared with

(25) Meier, T.; Chernyak, V.; Mukamel, S. *J. Phys. Chem. B* **1997**, *101*, 7332.

(26) Bakalis, L. D.; Knoester, J. *J. Phys. Chem. B* **1999**, *103*, 6620.

(27) van Oijen, A. M.; Ketelaars, M.; Köhler, J.; Aartsma, T. J.; Schmidt, J. *Science* **1999**, *285*, 400. (b) De Boer, S.; Wiersma, D. A. *Chem. Phys. Lett.* **1990**, *165*, 45.

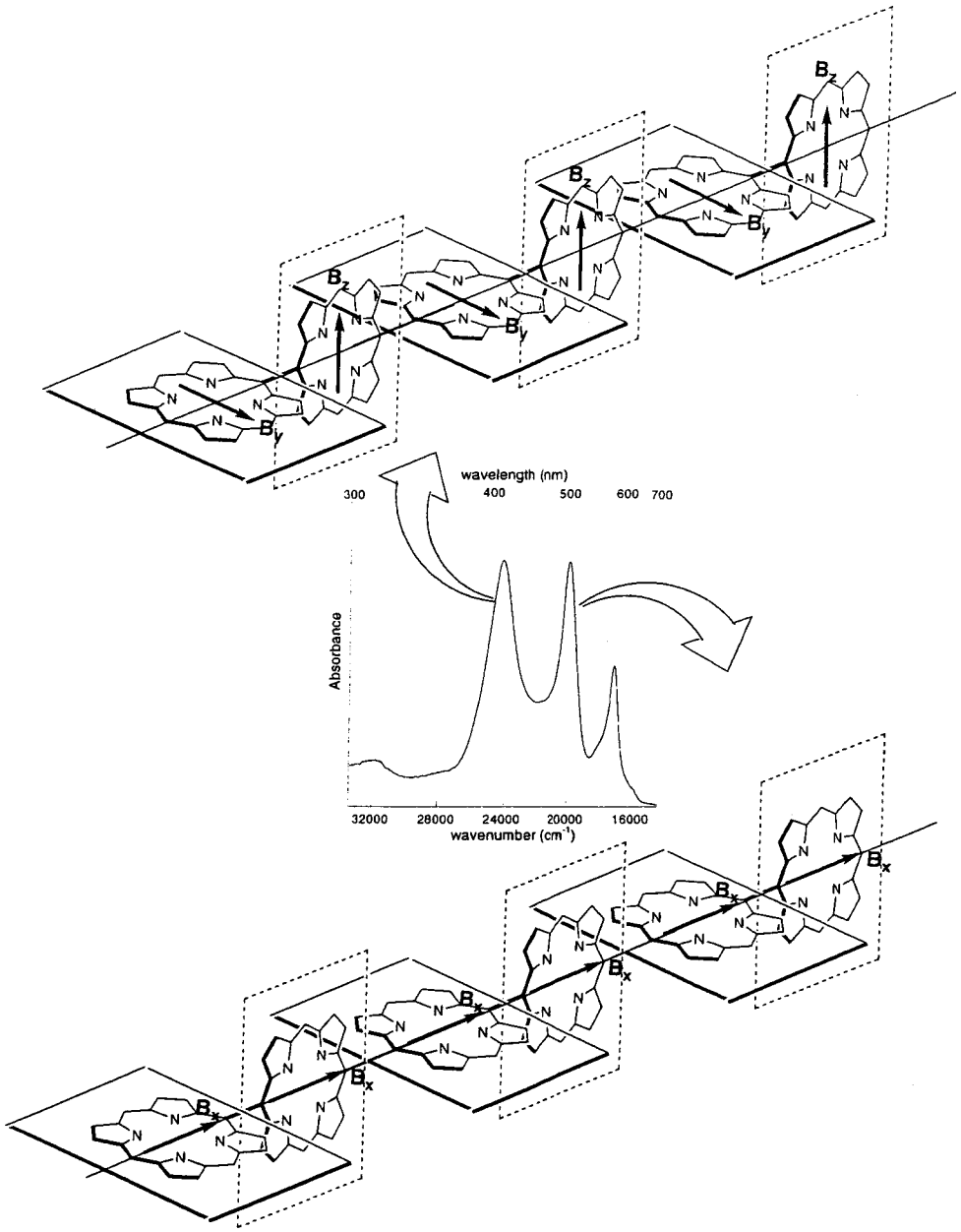

Figure 7. Representative assignment of the Soret band transition for Z6.

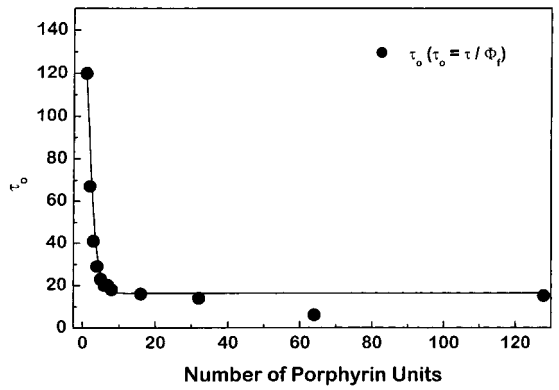

Figure 8. Plot of the number of porphyrin units in arrays vs the relative natural radiative times obtained by the fluorescence lifetimes and the relative fluorescence quantum yields of the porphyrin arrays.

longer center-to-center distance of ~20 Å between the nearest neighboring bacteriochlorophyll units embedded in protein matrix in LH1 and LH2 antenna complexes.

According to the formalism developed by Kakitani et al.,[28] the coherent length (N_c) can be estimated by eq 3,

$$N_c = \sqrt{\frac{3\pi^2|\Delta E_0|}{\gamma}} - 1 \qquad (3)$$

where γ represents the homogeneous broadening in the exciton level and can be estimated for chromophores in very similar environments by eq 4.

$$\gamma = \frac{1}{\pi(FC)_0} = \frac{\sqrt{4\pi\lambda k_B T}}{\pi} \qquad (4)$$

On the basis of ΔE_0 from eq 2 for the Soret band (S_2 state), the coupling strength for Q-band (S_1 state) has been estimated to be 270 cm^{-1}. By using the full width at half-height of the maximum absorption (fwhm), 236 cm^{-1} for the Q-band as the

(28) Kakitani, T.; Kimura, A.; Sumi, H. *J. Phys. Chem. B* **1999**, *103*, 6620.

value of γ, the N_c for S_1 state is determined to be ~5. When we consider a half of the Stokes shift as a λ in eq 4, the N_c for the S_1 state is determined to be ~7. These estimations are nicely fit with the experimental results. Applying this numerical calculation to the Soret band, we obtained $N_c = 15$ and 21 on the basis of fwhm and the Stokes shift, respectively. Thus, we can expect larger coherent length for the upper electronically excited S_2 state.

Internal Conversion Processes of the Porphyrin Arrays. There is a relatively large energy separation in metalloporphyrins between the S_2 and S_1 excited states, which appear as B- and Q-bands in UV−visible region. In addition, these two states are considered as a 50−50 admixture of two common excited electronic configurations $^1(a_{1u},e_g)$ and $^1(a_{2u},e_g)$ in accidental degeneracy and the energy surfaces of the S_1 and S_2 excited states are almost parallel. This definitely retards the $S_2 \rightarrow S_1$ intramolecular electronic internal conversion processes. Moreover, as suggested by the very intense B-band, the radiative process from S_2 to S_0 should be greatly accelerated (the strong S_2 oscillator emits). Thus as long as no T_1 state is located in energy between S_1 and S_2 states such as in diamagnetic metalloporphyrins, the S_2 fluorescence is anticipated. The S_1 state of Z1 is formed with ~1.6 ps time constant following Soret band excitation and decay to the ground state on a much slower time scale of ~2.64 ns. The observed, relatively slow 1.6 ps $S_2 \rightarrow S_1$ internal conversion for Z1 has been attributed to unfavorable Franck−Condon factors for nonradiative decay between parallel S_2 and S_1 potential energy surfaces, correlating with the relatively intense Q(1,0) transition for this complex; the optical properties of Z1 are consistent with similar Franck−Condon overlap of its S_2 and S_1 surfaces and the observation of a comparably slow internal conversion rate of 1.6 ps. The parallel excited-state surfaces, however, shift from the ground-state surface. In fact, the Franck−Condon overlap is so small that only a weak Q(0,0) band is observed in Z1.[29]

Formation of the emitting state occurs on a faster time scale for the porphyrin arrays than the constituent monomeric Z1. In the porphyrin arrays, the splitting of the component levels of the S_2 manifold establishes a band of intermediate levels between the state accessed by 400 nm excitation and the lowest emitting state. This provides a "ladder" for sequential relaxations between successive pairs of levels that are separated by energies much smaller than the S_2–S_1 gap of conventional porphyrin monomers and less strongly coupled porphyrin arrays (typically 7000−10 000 cm^{-1}). This facile internal conversion process for the porphyrin arrays as compared with Z1 monomer may be facilitated by improved Franck−Condon factors, with respect to the monomeric building blocks and/or from the fact that the highly split S_2 levels for the porphyrin arrays provide a large number of closely spaced intermediate states that enhance this process. For the quantitative analysis of the energy gap dependence on the internal conversion rates for the porphyrin arrays, we plot the $S_2 \rightarrow S_1$ internal conversion rates (~1.6 ps for Z1, ~0.3 ps for Z2, ~0.5 ps for Z3, and ~0.7 ps for Z4 and the limiting values of ~0.7 ps for longer oligomers) and the energy gap between the high-energy monomeric Soret band (S_2) and the low-energy exciton split Soret band (S_2'), because the $S_2' \rightarrow S_1$ internal conversion is believed to be much faster than the $S_2 \rightarrow S_2'$ process (Figure 9). The plot gives rise to an excellent linear correlation between the S_2–S_2' energy gap and the formation time of the lowest emissive S_1 state. The rate-determining step in the overall internal conversion processes upon photoexcitation to the S_2 states in the porphyrin arrays is likely to be the $S_2 \rightarrow S_2'$ internal conversion process. This argument can also be rationalized on the basis of the fluorescence polarization anisotropy measurement of the porphyrin arrays which shows that the S_2' states are the excitonic states being similar to the S_1 states in the transition dipole orientation in contrast with the monomeric localized electronic feature of the S_2 states. Hence the electronic coupling between S_2' and S_1 states is suggested to be much stronger as compared with that between S_2 and S_2' states.

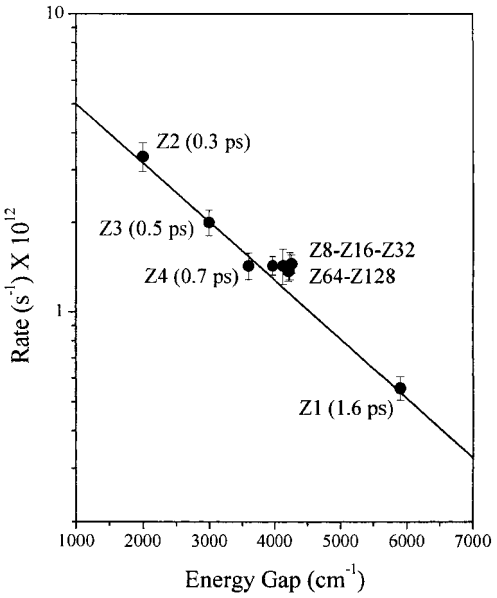

Figure 9. Plot of log(internal conversion rate) vs the energy gap between the high-energy Soret band and the low-energy exciton split Soret band ($S_2 - S_2'$) for porphyrin arrays. As for monomer Z1, the energy gap between the Soret and Q-bands ($S_2 - S_1$) was used.

Other Decay Processes of the Porphyrin Arrays. In the population dynamics of excitons in the *J*-aggregates, the excitation intensity dependence of the exciton lifetime observed at higher excitation densities was explained by the exciton−exciton annihilation. Likewise, the initial fast decay components of 1−4 ps time constants observed in longer porphyrin arrays under the high photoexcitation density are believed to arise from exciton−exciton annihilation processes. The initial fast decay components become increasingly manifest in longer porphyrin arrays than Z8 with an increase in the photoexcitation density. In the case of shorter porphyrin arrays than Z4, however, the temporal profiles remain relatively unchanged upon increasing the photoexcitation density. This experimental observation suggests that the two or more excitons are produced in the longer porphyrin arrays than four porphyrin units at higher excitation densities.

The subsequent decay/rise components of approximately 20−30 ps time constants after an initial fast rise in the fluorescence temporal profiles of the porphyrin arrays are believed to arise from the conversion of nonorthogonal S_1 state conformers to a perfectly orthogonally arranged emitting state of the porphyrin arrays.[23] The contribution by the heterogeneity of this series of samples to these processes is not so significant as indicated by the relatively small amplitudes of these components in the porphyrin arrays. We also cannot totally eliminate the possibility of aggregate or partially insoluble long arrays contributing to the excited-state relaxation dynamics of the porphyrin arrays. But the ^1H NMR signals of the long arrays are observed at nearly the same chemical shifts as those of the monomer and the dimer. These results seem to indicate that there is no significant

(29) Kasha, M. *Discuss. Faraday Soc.* **1950**, *9*, 14.

aggregation at the concentration for the ^{1}H NMR that is much higher than that for the UV−visible absorption measurement. Thus we think that the aggregation effect is not so significant in the energy relaxation dynamics of photoexcited porphyrin arrays. Both the amplitudes and the time constants of these components become larger as the number of porphyrin units in the arrays increases. This feature indicates that the conformational heterogeneity induced by the dihedral angle distribution between the adjacent porphyrins become manifest in longer porphyrin arrays. This feature can be further rationalized by a broader but unshifted high-energy Soret bands as the porphyrin arrays become longer, indicating that the contribution by the conformational heterogeneity increases.

Conclusions

In the fabrication of molecular photonic devices the rigid rodlike structure should be useful because the implementation of such molecules can be done in a more predictable manner. From a viewpoint of functional requirements, the arrays should have the very regular pigment arrangements which allow a facile incoherent hopping but do not result in the alteration of photophysical properties of the individual pigment leading to the formation of so-called energy sink. In these respects, the present *meso*−*meso*-linked porphyrin arrays are ideal, since they maintain the orthogonality between the adjacent porphyrin units, and consequently the conformational heterogeneity should be minimized. The directly linked porphyrin arrays up to 128 porphyrin units connected together linearly were successfully isolated, and their photophysical properties depending upon the length of the arrays were investigated by various time-resolved laser spectroscopic methods. Overall, the regularly arranged porphyrin arrays with ample electronic interactions will be promising as a light-harvesting photonic wire by transmitting singlet excitation energy rapidly over the array.

Acknowledgment. This work has been financially supported by the National Creative Research Initiatives Program of the Ministry of Science & Technology of Korea (D.K. and S.K.K.). The work at Kyoto was supported by Grant-in-Aids for Scientific Research from the Ministry of Education, Science, Sports, and Culture of Japan (No. 11223205) and by CREST (Core Research for Evolutional Science and Technology) of the Japan Science and Technology Corp. (JST).

Supporting Information Available: Transient absorption decay profiles, and a plot of ground-state energy change (Z2) depending on AMI calculated dihedral angle (PDF). This material is available free of charge via the Internet at http://pubs.acs.org.

JA0009976